Progress In Electromagnetics Research C, Vol. 115, 51–64, 2021

Performance Optimization of Dual-Feed UWB Annular Ring Antenna with Circular DGS and EBG for SAR Reduction

Mahesh Munde*, Anil Nandgaonkar, and Shankar Deosarkar

Abstract—The article presents the design of an Ultra-Wideband (UWB) annular ring antenna which operates over 1.5 GHz to 12 GHz and covers most of the bands of mobile communication (GSM 1800, 1900 and 2100, UMTS, Bluetooth (2.4 GHz), WLAN 2.4/3.5/5 GHz, and WiMAX 2.5/3.5/5.5 GHz). The antenna size is $40 \times 36.67 \times 1.6\,\text{mm}^3$, and an FR-4 substrate of permittivity 4.3 with loss tangent of 0.025 is used for fabrication. Circular defect in ground plane of annular ring is used to achieve UWB characteristics. A wideband mushroom type of Electromagnetic Band Gap (EBG) unit cell is designed which resonates at 2.3 GHz, and 8-unit cells are placed close to feeds of the annular ring patch where current density is more for 2.4 GHz, so as to reduce surface waves and ultimately to lower Specific Absorption Rate (SAR). SAR is evaluated with dual-feeds for single element and is lowered up to 83.64% for 1-gram of tissue mass.

1. INTRODUCTION

Antennas are the most prominent parts of any wireless communication system, so they must be designed with utmost care. Nowadays communication systems use multiple antennas for numerous applications which would cost more; also, there is often an issue with a specific absorption rate (SAR) diversity antenna operation, so the need has arisen to design single antenna that could serve multiple purposes. Multiband and ultra-wideband (UWB) antennas make carrier aggregation possible to increase transmission bandwidth which is the need of today [1]. Electromagnetic radiation absorbed by human tissue has to be given attention, since stringent guidelines are laid down by FCC, IEEE, and ICNIRP [2–4]. Guidelines are given for six minutes usage of mobile phones in talking mode, but humans are not restricting it, as cellular phones have become a vital part of our lives. Even though SAR value is 1.6 W/kg averaged in 1-gram of tissue and 2 W/kg averaged in 10-gram of tissue mass as per guidelines, for prolonged usage of mobile phone in talking mode it is advisable to have lower values of SAR. Also, multiple elements used simultaneously give rise to misleading SAR values, if SAR to peak location spacing ratio is not calculated and must be less than 0.3 if the spacing between elements is smaller than 5 cm [5].

Sievenpiper et al. were the first to propose high impedance surfaces characterized by LC equivalent circuit to minimize surface waves [6]. Zhu et al. proposed novel methods to evaluate the surface impedance of a mushroom type EBG unit cell [7]. Sarrazin et al. proposed an analytical model to predict reflection of incident waves in-phase. The reflected phase response of high impedance surface depends on the size of patches and gaps between them [8, 9] and offers zero reflection phase at resonant frequency [10]. Alam et al. proposed parasitic element and defective ground structure (DGS) for wideband antennas, and also used metamaterials for SAR reduction [11, 12]. Lee and Choi reduced back lobes using partial ground and improved radiation characteristics and front to back ratio of microstrip antenna [13]. Elsadek et al. used two spiral electromagnetic band gap (EBG) structures in the ground to

Received 24 April 2021, Accepted 13 August 2021, Scheduled 23 August 2021
* Corresponding author: Mahesh Munde (maheshmunde79@gmail.com).
The authors are with the Department of EXTC, Dr. Babasaheb Ambedkar Technological University, Maharashtra, India.

achieve multiband operation. Also, surface waves were suppressed using four different shapes, and the size reduction achieved is 70% [14, 15]. Prakash et al. used an EBG structure with rectangular defect in ground to achieve wide stopband [16]. Sultan et al. proposed a planar monopole and meander line to cover most of bands of handheld devices and used the EBG structure in [17], meander line and partial ground in [18] to reduce SAR. Ashyap et al. employed EBG and DGS for isolating human body from the wearable antenna and to broaden the bandwidth [19]. Chew presented an annular ring antenna and studied resonant modes, and TM_{12} mode gives good radiation, low Q factor, and high directivity [20]. El-khamy et al. varied ratio of outer to inner radii of the annular ring for exciting different modes [21]. Rawat and Sharma studied the behavior of an annular ring antenna over circular one and achieved better impedance bandwidth using partial ground [22]. Antonino-Daviu et al. used double feed for evading horizontal currents and improved bandwidth and polarization [23].

This article presents an extended work for optimizing size, achieving percentage reduction in SAR, and enhancing bandwidth to cover multiple bands for the work presented in [24, 25]. It aims at designing a small, compact UWB annular ring antenna. Wideband characteristics are achieved through an annular ring and better impedance matching through a circular defect in the ground. An EBG unit cell with 2.3 GHz resonant frequency is designed and placed on both sides of the stripline feed to minimize surface waves and reduce SAR considerably.

2. DESIGN OF DUAL-FEED UWB ANNULAR RING

The annular ring antenna uses TM_{mn} mode as field variations in Neumann's and Bessel's functions of order m are absent. The dominant mode is TM_{11}, and higher modes are excited to attain multiband resonance. The resonant frequency of circular antenna is given, referring to Eq. (1) [20, 21].

$$F_{mn} = \left(\frac{cX_{mn}}{2\pi r\sqrt{\varepsilon_{eff}}}\right) \tag{1}$$

where F_{mn} is the resonant frequency, X_{mn} the root for first order Bessel function, c the speed of light in free space, r the radius of the patch, and ε_{eff} the effective dielectric constant.

Equation (2) reveals resonant frequency for TM_{11}. Equation (3) gives ε_{eff}, and Equation (4) gives effective radius (r_e) considered due to fringing fields [26, 27].

$$F_{mn} = \left(\frac{1.8412C}{2\pi r_e\sqrt{\varepsilon_{eff}}}\right) \tag{2}$$

$$\varepsilon_{eff} = \left(\frac{\varepsilon_r+1}{2}\right) + \left(\frac{\varepsilon_r-1}{2}\right)\left(1+\frac{12h}{w}\right)^{-\frac{1}{2}} \tag{3}$$

$$r_e = r\left(1+\frac{2h}{\pi r\varepsilon_r}\left(\ln\left(\frac{\pi r}{2h}\right)+1.7726\right)\right)^{\frac{1}{2}} \tag{4}$$

where ε_r is the relative permittivity, h the substrate height, and w the width.

Annular ring antenna is significantly smaller than circular or rectangular antenna and shows greater input impedance, if it is operated in fundamental mode. The ratio of outer and inner radii regulate separation among the modes. An appropriate choice of the radii broadens bandwidth [21]. The basic approximation of Bessel function gives rectified radius revealed by Equation (5) and is substituted in Equation (6) to get resonant frequency for the dominant mode [27]. Real radius of an annular ring is '$(b-a)$', and b and a are outer and inner radii, respectively.

$$(b-a)_e = (b-a)\left\{1+\frac{2h}{\pi\,(b-a)_e\,\varepsilon_r}\left[\ln\left(\frac{\pi\,(b-a)}{2h}\right)+1.7726\right]\right\}^{\frac{1}{2}} \tag{5}$$

$$f_r = \left(\frac{1.8412\,C}{2\pi\,(b-a)_e\,\sqrt{\varepsilon}_r}\right) \tag{6}$$

f_r is the resonant frequency, and $(b-a)_e$ is the rectified radius.

Performance of antenna is improved by varying width of the annular ring. The ratio of radii is varied in the range of 2.5 to 3 and is optimized at 2.7, so broadening of the bands occurs, and defect

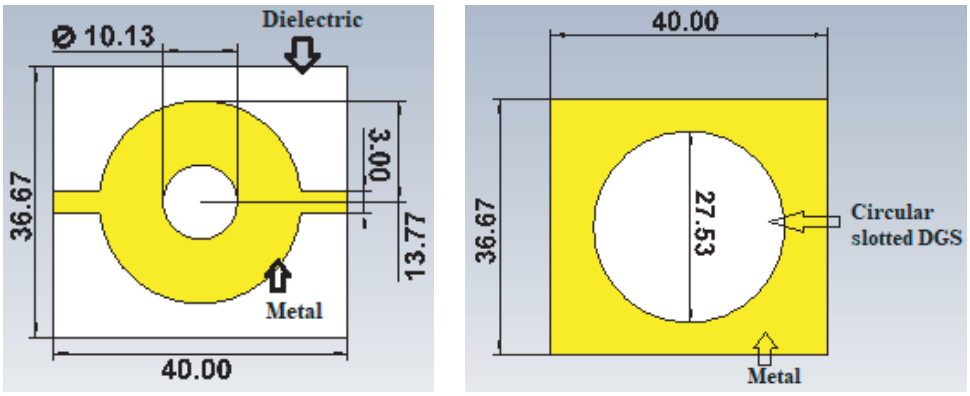

Figure 1. Designed UWB annular ring antenna. All dimensions depicted in figure are in mm.

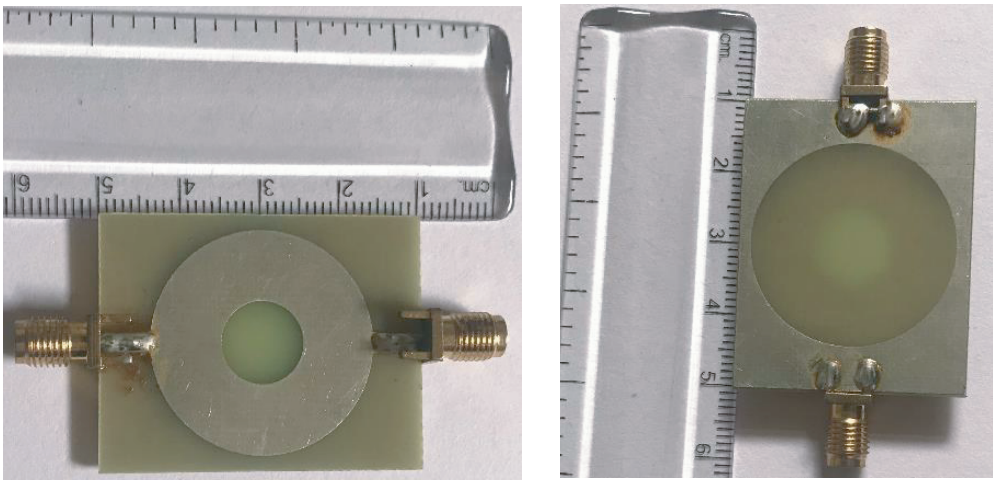

Figure 2. Fabricated UWB annular ring antenna.

in the ground produces further widening of the bands. Designed and fabricated dual-feed annular ring antennas with a circular defect in ground are shown in Fig. 1 and Fig. 2. Dual-feed facilitates enhancing gain and reducing SAR value, and single feed with 1 W input power produces higher SAR. When dual-feeds on opposite sides are used with half (0.5 W) input power at each port with opposite phase excitation, the gain adds constructively. Hence, isolation among ports as in MIMO is not required; also, it produces lower SAR value as discussed in detail and presented in [24].

Figure 3 shows simulated and measured S-parameters for antenna over 1.5 GHz–12 GHz, when both the ports are excited simultaneously with 0.5 W input power keeping the amplitude same and phase 0° at port 1 and 180° at port 2. The antenna gives reflection coefficient ($S_{11} < -10$ dB) for all the desired bands. Measured and simulated results show variation due to fabrication accuracy and excessive soldering material on the microstrip feed.

3. SAR EVALUATION

Figure 4 presents SAR evaluation method for dual-feed UWB annular ring antenna in which a human head along with handset case and hand model from CST-MW studio are used. The annular ring antenna is fixed in mobile handset case, and the port is fed with 1 W of power as an excitation signal, as in transmit mode the antenna uses power up to 1 W. The evaluated value of SAR will be the peak value. The detailed information on properties used by SAM phantom model [28] with hand and handset is listed in Table 1 [29].

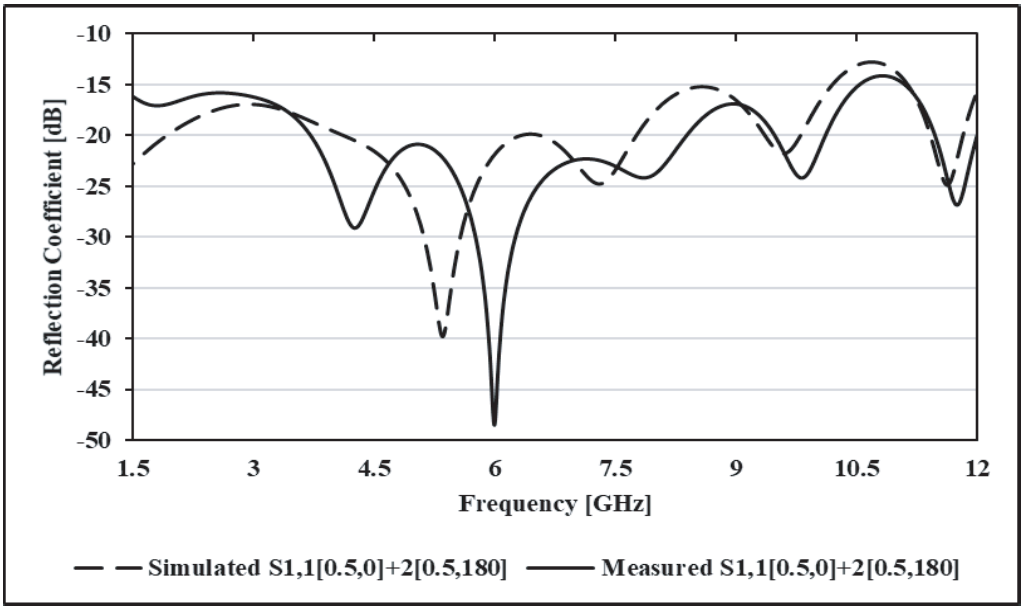

Figure 3. Reflection coefficient v/s frequency for antenna without EBG.

Figure 4. Antenna fixed in handset along with hand and head.

UWB antennas are operated over a large range of frequencies and support different applications, but when being used for mobile handset they must comply with the guidelines given by FCC and IEEE C95.3. The dual-feed UWB annular ring antenna gives higher value of SAR than the value set in guidelines at 2.4 GHz band which is presented in Table 2. Surface current distribution is analyzed at 2.4 GHz by providing input at port 1 and terminating port 2 with 50 Ω. It is evident that due to surface current, surface waves are generated near the feed line strips for all the desired bands, but the surface current is eventually more for 2.4 GHz frequency which is depicted in Fig. 5. EBG structure when incident with waves at any angle and any polarization will reflect waves at that frequency where reflection phase is zero degrees, and consequently waves are reflected from ground and are radiated at an angle of 90°.

Table 1. Parameters of phantom model with hand and handset.

Model parts	Material type	Conductivity	Relative Permittivity
Hand	Normal	1	20
Plastic Case	Normal	-	2.5
LCD Film	Normal	-	4.78
Rubber pads	Normal	0.005	3.5
SAM Fluid	Normal	1.42	40
SAM Shell	Normal	0.0016	3.7

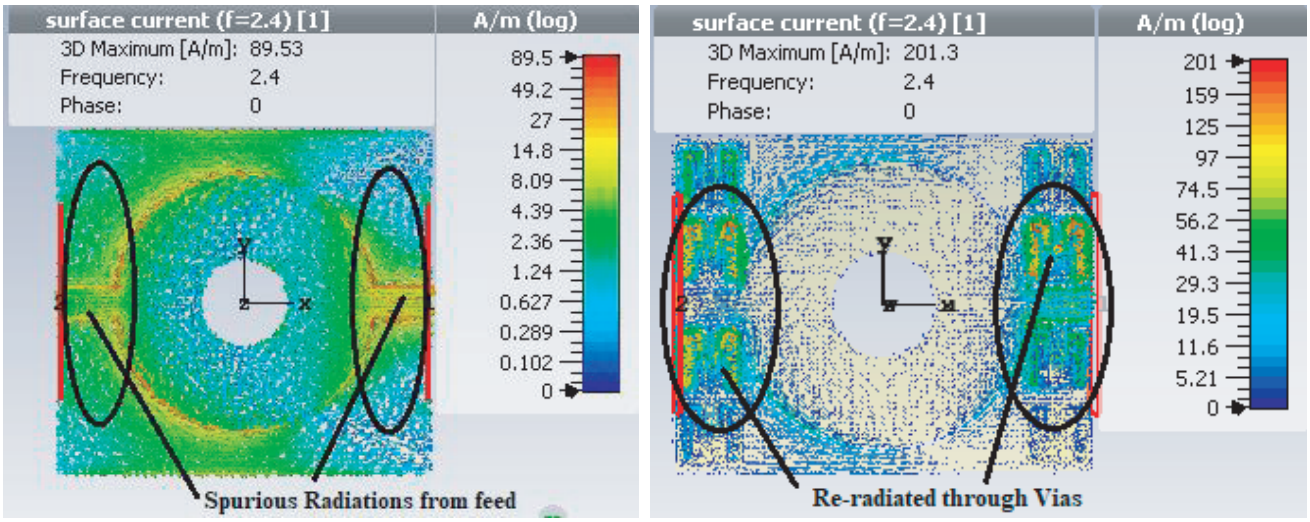

(a) (b)

Figure 5. Surface current distribution at 2.4 GHz for dual-feed UWB annular ring antenna with and without EBG. (a) Without EBG. (b) With EBG.

4. UNIT CELL MODELLING AND ANALYSIS

To minimize surface waves for a reduction in SAR, EBG unit cells must be placed near feed lines as spurious radiations are more near feed. Planar EBG unit cells must be used on ground plane or with the multi-layer structure for effective suppression of surface waves and spurious backward radiation towards human head. Mushroom type unit cells can be used on the top surface along with the main radiating patch to enhance performance in terms of impedance bandwidth. Slotted unit cell with shorting vias is designed and operated over a wideband. Figs. 6(a) and (b) show the characterization of unit cell by means of reflection phase method, where periodic boundary conditions are applied in x and y directions along with plane wave incident in z-direction. This method is more convenient as it analyses reflected E-field with respect to incident E-field for a perfect magnetic conductor. The result gives reflection coefficient as one and phase as 0°. Reflection phase is achieved which is a function of frequency and varies from +180° to −180°; this also gives stop bandgap bandwidth between +90° and −90° for plane wave incidence [30].

Theoretically lumped LC model gives an analysis of EBG unit cell, where vias are represented by L, and gap between unit cells is represented by C, which are dependent on the geometry of the unit cell. Fig. 7 shows LC lumped model, and for designing a unit cell at 2.4 GHz, λ calculated is 125 mm and acts as a reference for the dimension of unit cell. These values are determined using Equations (7),

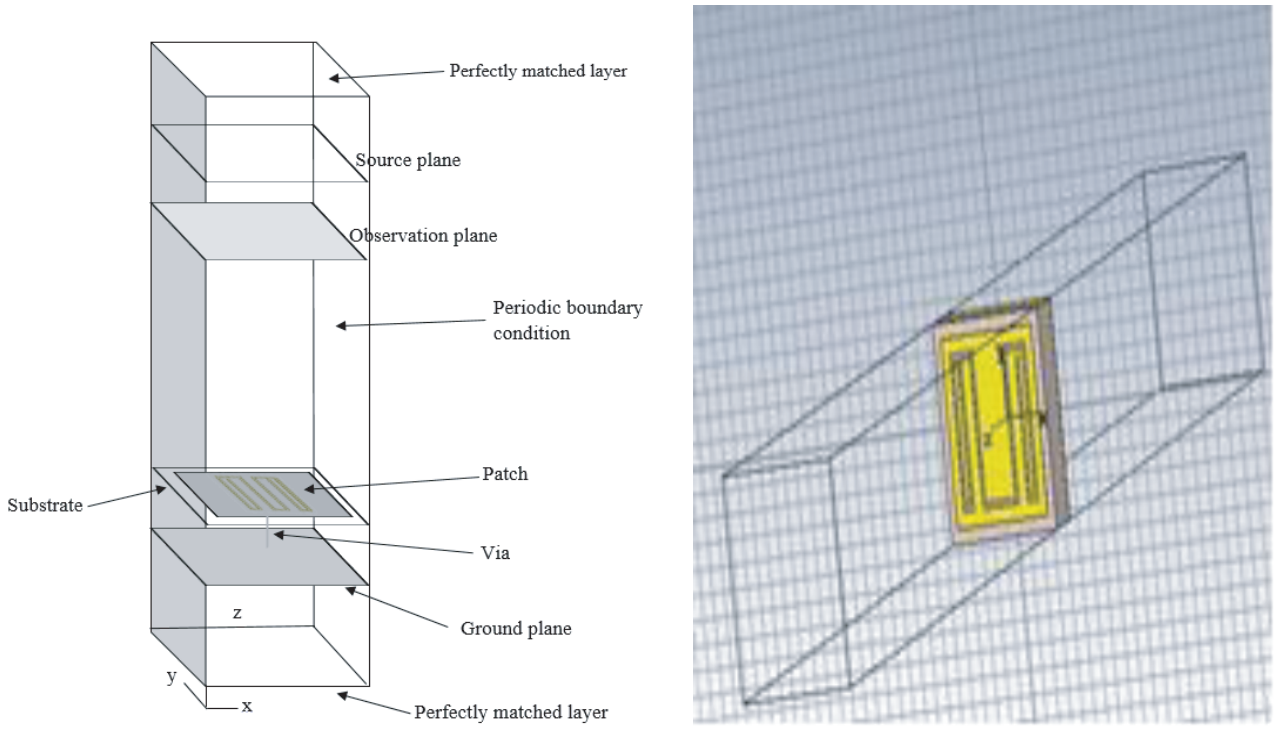

Figure 6. Reflection phase method for characterization of EBG unit cell.

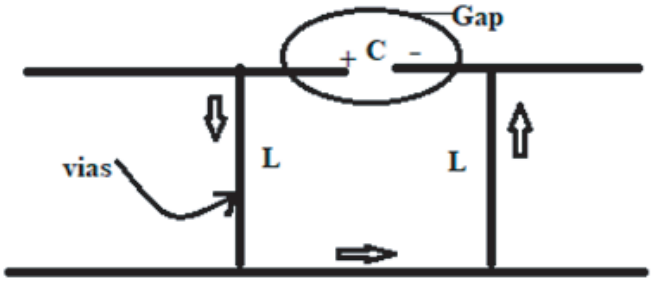

Figure 7. Lumped LC model.

(8), and (9) below.

$$f_r = \left(\frac{1}{2\pi\sqrt{LC}}\right) \tag{7}$$

$$L = \mu h \tag{8}$$

$$C = \left(\frac{w\varepsilon_0\left(1+\varepsilon_r\right)}{\pi}\right)\cosh^{-1}\left(\frac{w+g}{g}\right) \tag{9}$$

where f_r is the resonant frequency of unit cell, L the inductance, C the capacitance, μ the permeability, h the thickness of substrate, w the width of unit cell, g the gap between unit cells, ε_r the relative permittivity, and ε_0 the permittivity of free space.

The capacitance between adjacent copper patches is calculated, whereas inductance results from the current loop. At low frequency, the impedance becomes inductive and assists TM surface waves. At high frequency, it turns out to be capacitive due to gaps between unit cells and supports TE surface

waves. At resonant frequency EBG will impose its stopband characteristics as the surface offers the highest impedance [30].

Design parameters for EBG unit cell required are very small and are in proportion to reference wavelength; width is 0.048λ; the gap between unit cells is 0.008λ; dielectric constant is 4.3; radius of via is 0.0048λ; substrate height is 0.012λ.

Figure 8 depicts an EBG unit cell along with dimensions, and Fig. 9 shows the phase reversal of the unit cell for plane wave incidence at 0° which is almost constant for all incident angles. It is evident that reflection phase crosses 0° at 2.328 GHz which is close to the 2.4 GHz band and exhibits stopband. The stopband bandwidth computed is 2.29 GHz for reflection phase characteristic in between +90° and −90° which is very wide. Also in the article [31], reflection phase is estimated in between $90° \pm 45°$.

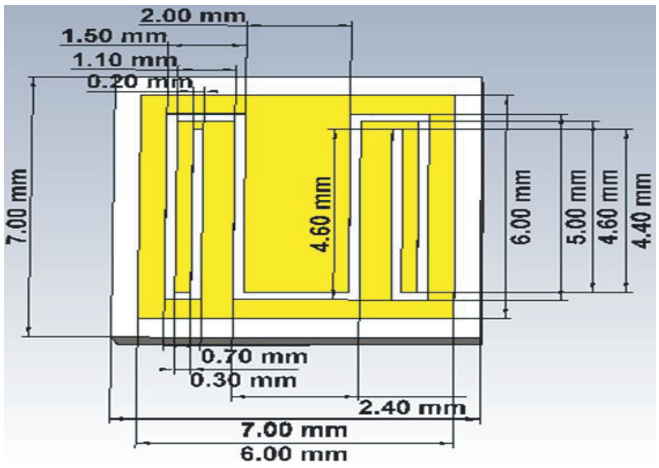

Figure 8. EBG unit cell.

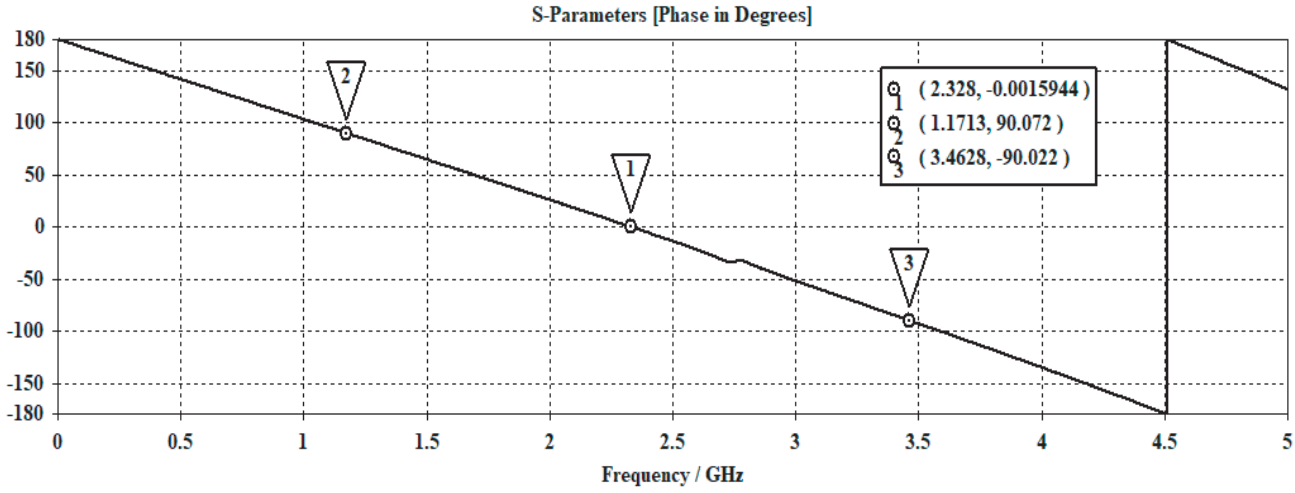

Figure 9. Reflection phase characteristic of unit cell for plane wave at normal incidence.

5. DUAL-FEED UWB ANNULAR RING WITH EBG STRUCTURE AND SAR

Figure 10 shows a fabricated prototype of dual-feed UWB annular ring antenna with EBG unit cells placed on both sides of feeds, so as to minimize surface loss at 2.4 GHz band. The center frequency of the unit cell is 2.328 GHz and will offer its stopband feature in the range of 1.17 GHz to 3.46 GHz.

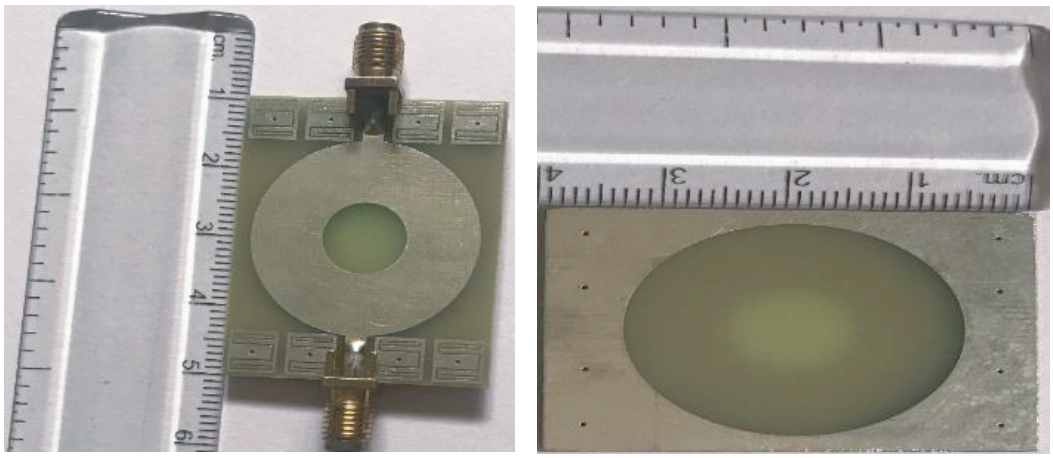

Figure 10. Fabricated UWB annular ring antenna with EBG.

Figure 11 depicts measured and simulated S-parameters for the UWB annular ring antenna with EBG, which is placed inside handset over 1.5 GHz–12 GHz, and the ports are excited simultaneously with 0.5 W input. The settings used for phase are like those used earlier for the antenna without EBG. It is evident that the reflection coefficient for the entire UWB is less than −10 dB and has more variation in values for corresponding stopband. The variation in reflection coefficient can be witnessed from Fig. 11, and deterioration is almost 75% for 5.5 GHz band whereas for other bands of interest it is around 10%. Fig. 12 depicts measured and simulated gains in dBi for both the antennas (with and without EBG) over the entire band by exciting port 1 with 1 W and terminating port 2 with 50 Ω terminator. Gain attains the maximum value of 4.32 dBi for annular ring antenna without EBG and 4.55 dBi for the annular ring antenna with EBG. It is evident that the gain is slightly enhanced by 6.3%

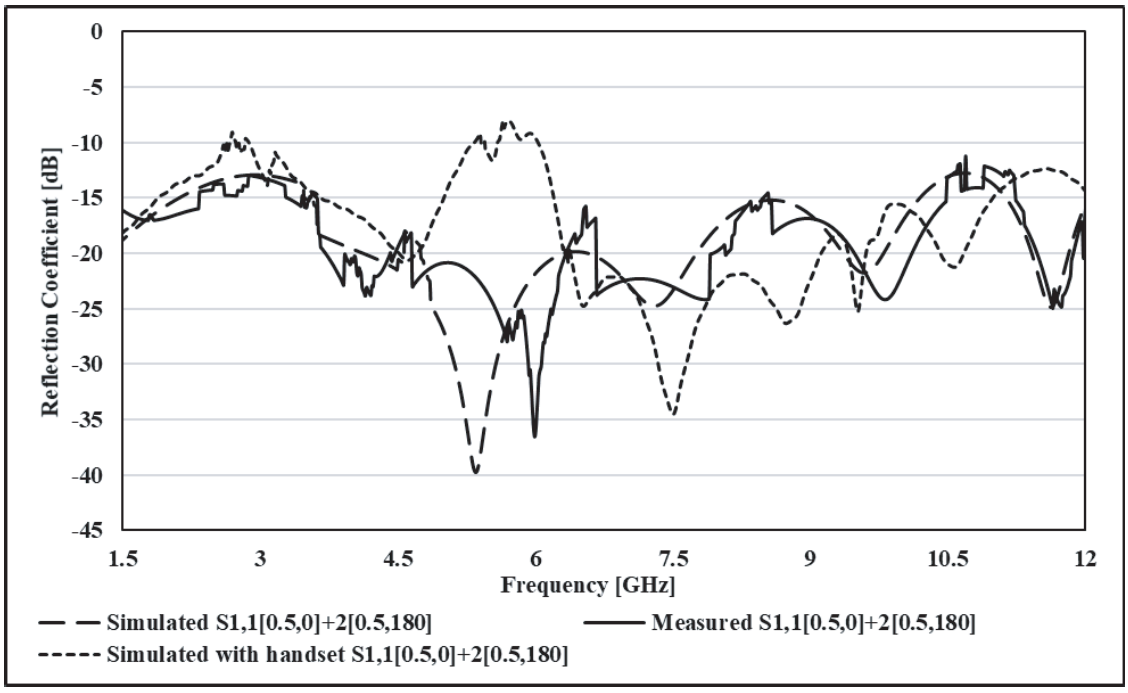

Figure 11. Reflection coefficient v/s frequency for antenna with EBG.

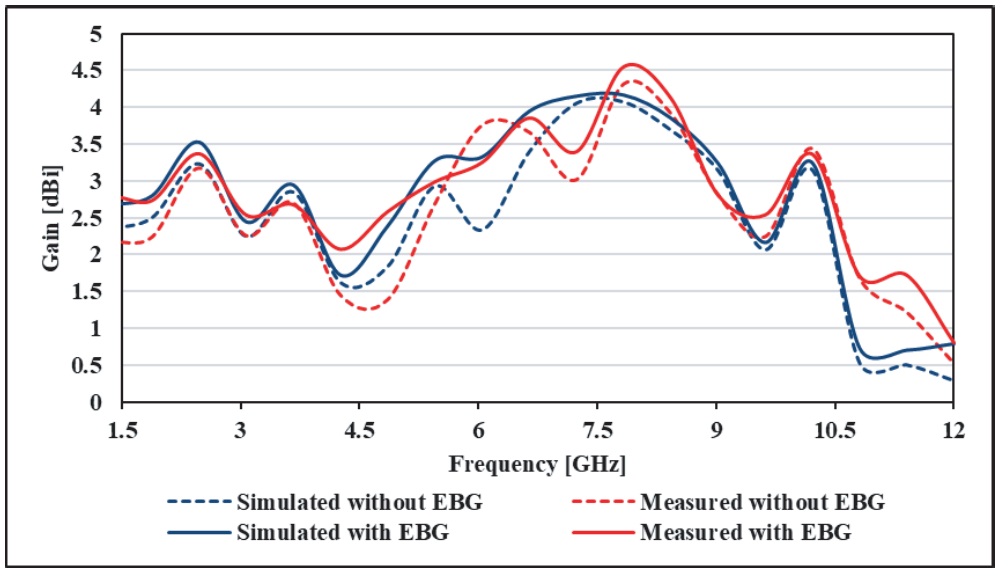

Figure 12. Variation in maximum gain for antenna without EBG.

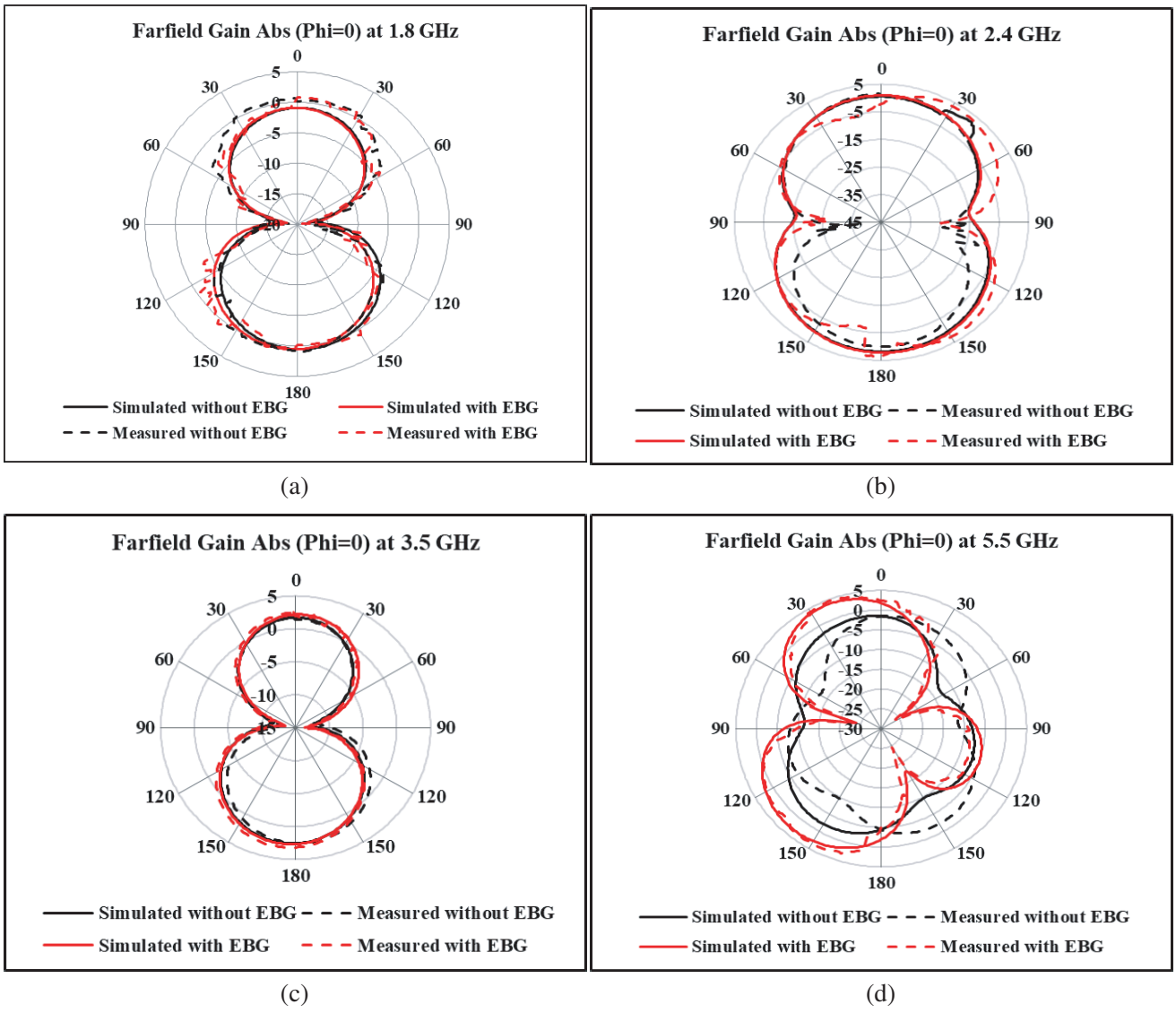

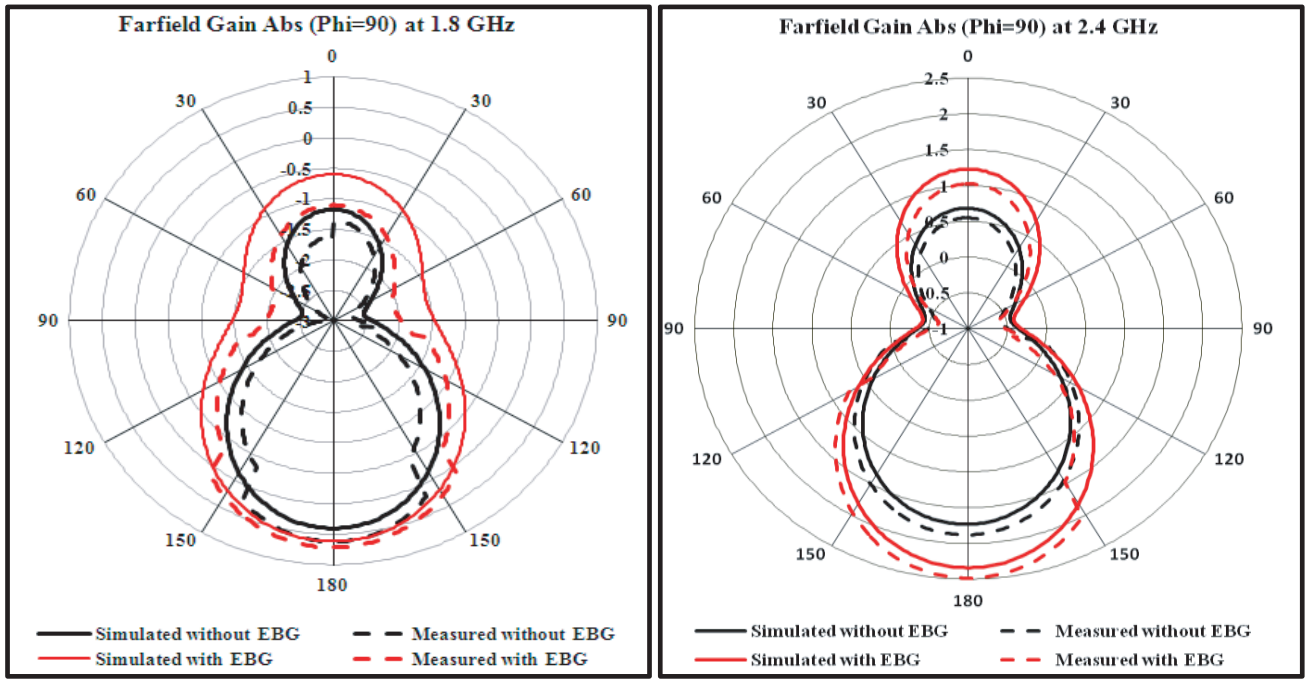

(e) (f)

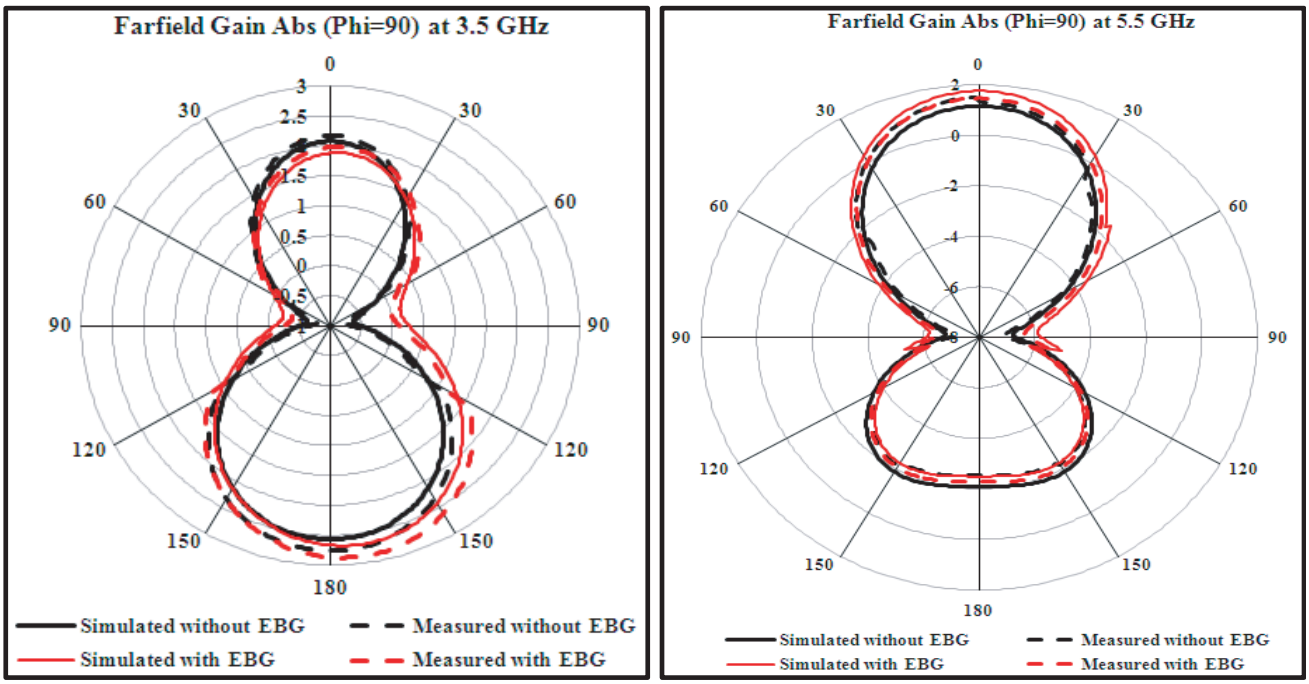

(g) (h)

Figure 13. (a)–(h) Simulated and measured radiation patterns of both the antennas (with and without EBG).

at 2.48 GHz when patch is used with EBG. Reflection coefficient and gain of both the configurations are characterized over the entire band from 1.5 GHz to 12 GHz, but radiation patterns are depicted for the specific bands of interest (1.8 GHz, 2.4 GHz, 3.5 GHz, and 5.5 GHz).

Figures 13(a)–(d) and (e)–(h) depict simulated and measured radiation patterns of both the

antennas (with and without EBG) at Φ_0 and Φ_{90}, respectively. It is witnessed that in both the cases, radiation patterns are similar at 1.8 GHz, 2.4 GHz, and 3.5 GHz, whereas slightly differ at 5.5 GHz at Φ_0.

It is evident from Table 2 that due to the use of EBG unit cells, SAR values at all desired frequency bands are reduced drastically for 1 gram and 10 gram of tissue mass except at 3.5 GHz. The major concern is for 2.4 GHz band as the value of SAR evaluated which is 1.904 for 1 gram tissue and higher than the value set in guidelines of FCC, but when EBG structure is employed with a UWB annular ring antenna the value of SAR is decreased by 82.86%. Comparison of SARs for with and without EBG is given in Table 2 for all the frequencies. Table 3 presents the comparison of SAR with existing literature, when the antenna uses frequency selective surfaces.

Table 2. Comparison of SAR [W/kg] for dual-feed UWB annular ring antenna.

Frequency [GHz]	Without EBG		With EBG		% Reduction in SAR	
	1 g	10 g	1 g	10 g	1 g	10 g
1.8	0.730	0.044	0.12	0.11	83.64	74.60
2.4	1.904	0.966	0.326	0.29	82.86	69.87
3.5	1.277	0.641	0.77	0.62	39.70	3.12
5.5	0.824	0.248	0.188	0.070	77.18	71.77

6. COMPARISON OF PROPOSED WORK WITH EXISTING LITERATURE

Table 3. Comparison of SAR [W/kg] at different frequencies [GHz].

Reference No. and Year	1.8		2.4		3.5		5.5	
	1 g	10 g	1 g	10 g	1 g	10 g	1 g	10 g
[32], 2017	0.452	0.237	1.1	0.925	0.67	0.384	0.75	0.249
[33], 2018	-	-	2.48	0.7	-	-	3.33	0.71
[24], 2020	0.311	0.189	0.218	0.12	0.229	0.099	-	-
[34], 2020							0.724	-
[35], 2021	-	-	2.49	-	2.49	-	1.645	-
[36], 2021	1.26	-	1.67	-	-	-	-	-
[37], 2021					0.25	0.071	0.7	0.171
proposed	0.1195	0.113	0.3262	0.291	0.77	0.621	0.188	0.070

7. CONCLUSION

Band broadening can be achieved by introducing defect in ground plane (DGS). Size reduction and circular defect converts multiband antenna into UWB antenna operation wise, also reducing SAR to some extent. Many single band antennas can be replaced by multiband or wideband antenna which will serve the purpose and reduce the overall cost of the product. When ports 1 and 2 of the dual-feed annular ring antenna are excited with 0.5 W input power, and phase of 0° and 180° respectively, it produces low SAR. Mushroom type EBG cells are placed on the top surface near the feed to reduce surface waves, and additionally SAR is reduced up to 83.64%. Standards quote acceptable value of SAR must be less than 1.6 W/kg for 1-gram averaged tissue mass for 6 minutes in talking mode, but extensive use of mobile phones for prolonged duration in talking mode can severely affect human health; it is therefore beneficial to have low SAR values.

ACKNOWLEDGMENT

Authors would like to thank Mr. Anirudhda Kulkarni (Team Lead) and Mukund Bhople (RF Test Engineer), Cyronics Instruments Pvt. Ltd. Pune, India, for providing set-up to carry out the measurements.

REFERENCES

1. Campbell, D. and C. J. Reddy, "Antenna design considerations for LTE enabled tablets," *2015 IEEE International Symposium on Antennas and Propagation & USNC/URSI National Radio Science Meeting*, 1140–1141, Vancouver, BC, 2015.
2. US Federal Communication Commission, Office of Engineering and Technology, "Evaluating compliance with FCC-specified guidelines for human exposure to radio radiofrequency radiation," *OET Bulletin 65*, Washington, DC, 1997.
3. Institute of Electrical and Electronic Engineers (IEEE), IEEE C95.1-2005, *Standards for Safety Levels with Respect to Human Exposure to Radio Frequency Electromagnetic Fields*, IEEE Press, New York, 2005.
4. International Commission on Non-Ionizing Radiation Protection (ICNIRP), "Guidelines for limiting exposure to time-varying electric, magnetic, and electromagnetic fields (up to 300 GHz)," *Health Physics*, Vol. 74, 494–522, 1998.
5. Zhao, K., S. Zhang, Z. Ying, T. Bolin, and S. He, "SAR study of different MIMO antenna designs for LTE application in smart mobile handsets," *IEEE Transactions on Antennas and Propagation*, Vol. 61, No. 6, 3270–3279, Jun. 2013.
6. Sievenpiper, D., L. Zhang, R. F. J. Broas, N. G. Alexopolous, and E. Yablonovitch, "High-impedance electromagnetic surfaces with a forbidden frequency band," *IEEE Transactions on Microwave Theory and Techniques*, Vol. 47, No. 11, 2059–2074, Nov. 1999.
7. Zhu, Y., A. Bossavit, and S. Zouhdi, "Surface impedance models for high impedance surfaces," *Appl. Phys. A*, Vol. 103, 677–683, 2011.
8. Sarrazin, J., A. C. Lepage, and X. Begaud, "Dual-band artificial magnetic conductor," *Appl. Phys. A*, Vol. 109, 1075–1080, 2012.
9. Sarrazin, J., A. Lepage, and X. Begaud, "Circular high-impedance surfaces characterization," *IEEE Antennas and Wireless Propagation Letters*, Vol. 11, 260–263, 2012.
10. Linot, F., R. Cousin, X. Begaud, and M. Soiron, "Design and measurement of high impedance surface," *Proceedings of the Fourth European Conference on Antennas and Propagation*, 1–4, Barcelona, 2010.
11. Alam, T., M. Faruque, and M. Islam, "Printed circular patch wideband antenna for wireless communication," *Informacije Midem Journal of Microelectronics Electronic Components and Materials*, Vol. 44, 212–217, 2014.
12. Alam, T., et al., "Specific Absorption Rate (SAR) analysis using plastic substrate based negative indexed metamaterial shielding," *2017 International Conference on Electrical, Computer and Communication Engineering (ECCE)*, 619–622, Cox's Bazar, 2017.
13. Lee, H. and W. Choi, "Effect of partial ground plane removal on the radiation characteristics of a microstrip antenna," *Wireless Engineering and Technology*, Vol. 4, No. 1, 5–12, 2013.
14. Nashaat, D., H. Elsadek, E. Abdallah, H. Elhenawy, and M. F. Iskander, "Multiband and miniaturized inset feed microstrip patch antenna using multiple spiral-shaped defect ground structure (DGS)," *2009 IEEE Antennas and Propagation Society International Symposium*, 1–4, Charleston, SC, 2009.
15. Elsheakh, D., H. Elsadek, E. Abdallah, M. Iskander, and H. El-Hennawy, "Investigated new embedded shapes of electromagnetic bandgap structures and via effect for improved microstrip patch antenna performance," *Progress In Electromagnetics Research B*, Vol. 20, 91–107, 2010.

16. Prakash, P., M. P. Abegaonkar, L. Kurra, A. Basu, and S. K. Koul, "Compact Electromagnetic Bandgap (EBG) structure with defected ground," *IETE Journal of Research*, Vol. 62, No. 1, 120–126, 2016.
17. Sultan, K., H. Abdullah, E. Abdallah, and E. Hashish, "Low SAR, compact and multiband antenna for mobile and wireless communication," *The 2nd Middle East Conference on Antennas and Propagation*, 1–5, Cairo, 2012.
18. Sultan, K., H. Abdullah, and E. Abdallah, "Low SAR, simple printed compact multiband antenna for mobile and wireless communication applications," *International Journal of Antennas and Propagation*, Vol. 2014, 1–9, 2014.
19. Ashyap, A. Y. I., et al., "Robust and efficient integrated antenna with EBG-DGS enabled wide bandwidth for wearable medical device applications," *IEEE Access*, Vol. 8, 56346–56358, 2020.
20. Chew, W., "A broad-band annular-ring microstrip antenna," *IEEE Transactions on Antennas and Propagation*, Vol. 30, No. 5, 918–922, Sept. 1982.
21. El-khamy, S., R. El-Awadi, and E. A. El-Sharrawy, "Simple analysis and design of annular ring microstrip antennas," *IEE Proceedings H — Microwaves, Antennas and Propagation*, Vol. 133, No. 3, 198–202, 1986.
22. Rawat, S. and K. Sharma, "Annular ring microstrip patch antenna with finite ground plane for ultra-wideband applications," *International Journal of Microwave and Wireless Technologies*, Vol. 7, No. 2, 179–184, 2015.
23. Antonino-Daviu, E., M. Cabedo-Fabres, M. Ferrando-Bataller, and A. Valero-Nogueira, "Wideband double-fed planar monopole antennas," *Electronics Letters*, Vol. 39, No. 23, 1635–1636, Nov. 2003.
24. Munde, M., A. Nandgaonkar, and S. Deosarkar, "Dual feed wideband annular ring microstrip antenna with circular DGS for reduced SAR," *Progress In Electromagnetics Research B*, Vol. 88, 175–195, 2020.
25. Munde, M., A. Nandgaonkar, and S. Deosarkar, "Low specific absorption rate antenna using electromagnetic band gap structure for long term evolution band 3 application," *Progress In Electromagnetics Research M*, Vol. 80, 23–34, 2019.
26. Garg, R., *Microstrip Antenna Design Handbook*, Boston, Artech House, 2001.
27. Balanis, C., *Antenna Theory: Analysis and Design*, Wiley India, New-Delhi, Reprint, 2016.
28. ITIS Foundation, "Dielectric properties of body tissues," https://itis.swiss/virtual-population/tissue-properties/ database/dielectric-properties.
29. Faruque, M. R. I., M. I. Hossain, N. Misran, M. Singh, and M. T. Islam, "Metamaterial-embedded Low SAR PIFA for cellular phone," *PLoS ONE*, Vol. 10, No. 11, e0142663, 2015.
30. Yang, F. and Y. Rahmat-Samii, *Electromagnetic Band Gap Structures in Antenna Engineering*, Cambridge University Press, New York, 2009.
31. Saleh, G., K. Solbach, and A. Rennings, "EBG structure for low frequency applications," *The 7th German Microwave Conference*, 1–4, Ilmenau, 2012.
32. Ahmed, M. I., M. F. Ahmed, and A. H. A. Shaalan, "SAR calculations of novel wearable fractal antenna on metamaterial cell for search and rescue applications," *Progress In Electromagnetics Research M*, Vol. 53, 99–110, 2017.
33. Wang, M., et al., "Investigation of SAR reduction using flexible antenna with metamaterial structure in wireless body area network," *IEEE Transactions on Antennas and Propagation*, Vol. 66, No. 6, 3076–3086, Jun. 2018.
34. Badugu, P., M. Boddapati, S. Munuswamy, A. Tirunagari, V. Manikonda, and V. Poluri, "Windmill-shaped antenna with artificial magnetic conductor-backed structure for wearable medical applications," *Int. J. Number Model El.*, Vol. 33, e2757, 2020.
35. Rosaline, S. I., "A triple-band antenna with a metamaterial slab for gain enhancement and Specific Absorption Rate (SAR) reduction," *Progress In Electromagnetics Research C*, Vol. 109, 275–287, 2021.

36. Imran, A. I., T. A. Elwi, and A. J. Salim, "On the distortionless of UWB wearable hilbert-shaped metamaterial antenna for low energy applications," *Progress In Electromagnetics Research M*, Vol. 101, 219–239, 2021.
37. Mahmood, S. N., A. J. Ishak, T. Saeidi, A. C. Soh, A. Jalal, M. A. Imran, and Q. H. Abbasi, "Full ground ultra-wideband wearable textile antenna for breast cancer and wireless body area network applications," *Micromachines (Basel)*, Vol. 12, No. 3, 322, Mar. 19, 2021.